

Reduction of the Ripple of Torque in the Brushless Permanent Magnet Motor using the Optimal Design of the Motor Structure

A. Mousaei¹, S. Aziz Mohammad Abadi

¹ Faculty of Electrical and Computer Engineering, University of Tabriz, Tabriz; a.mousaei@tabrizu.ac.ir

² Faculty of Electrical Engineering, University of Pisa, Italy; Azimisah@gmail.com

Abstract

In this article, the calculation of momentary electromagnetic torque in a brushless shaft permanent magnet motor has been done using Lorentz force theory. In this method, the anti-motor voltage and phase current are used and a new method for calculating the different harmonics of the anti-motor voltage has been presented using an analytical method. The results of the presented analytical method have been evaluated using the finite element software and there is a good match between the presented analytical method and the finite element method. The calculation time in the presented analytical method is much less than the calculation time of Alman software. Finally, by using the analytical method, some geometrical parameters of the motor have been optimized with the aim of reducing the ripple torque.

Keywords: BLDC motor, AFPM motor, Electromagnetic torque, Torque ripple, Electric Vehicle.

Introduction

Recently, brushless permanent magnet servo motors have become a serious competitor for brushed motors in industrial applications. Due to its high-power density, low rotational inertia, and good dynamic performance, the brushless permanent magnet servo motor has been widely used in various applications [1] and [2]. Noise and vibration reduce the stability of the servo system and make it difficult to use it for industrial applications with high precision.

Brushless permanent magnet motors are divided into two categories: permanent magnet synchronous motors with sinusoidal current feeding or PMSM and brushless permanent magnet motor with rectangular current feeding or BLDC. In the ideal case, the anti-motor voltage in PMSM is sinusoidal and in BLDC the anti-motor voltage is trapezoidal. If the conditions are ideal in both methods and the waveforms of current and voltage are what is expected, in both cases the production torque will be without fluctuations, which is desirable in many applications. In any case, in operation, the counter-motive voltage in permanent magnet motors is not completely sinusoidal or perfectly trapezoidal, and due to mechanical errors and design limitations, it is almost impossible to produce the desired counter-motive voltage waveform.

Two-way spindle permanent magnet motors are among the brushless permanent magnet motors, which have significant advantages compared to normal permanent magnet motors [1-6] due to features such as high torque

to weight and high efficiency. It shows the motors that have a middle stator structure without grooves.

It has two components, one fixed component or average torque, which is useful torque, and the other is fluctuating torque, which causes torque fluctuations [9]. The factors of producing fluctuating torque can be divided into two categories: structural factors of the motor and factors arising from it. The sources of generating the oscillating torque caused by the motor structure are: [10]

- The torque of the teeth, which is created by the interaction between the variable armature grooves and the magnetic flux of the rotor magnets.
- The reluctance torque that is created due to the inequality of the d-axis and q-axis torques.
- The harmonic electromagnetic torque due to the non-ideal distribution of the magnetic flux density in the air gap is non-sinusoidal in PMSM and not trapezoidal in BLDC.

The sources of generating the oscillating torque that originates from the power supply can be referred to the ripple in the power supply and the commutation of the phase current.[10]

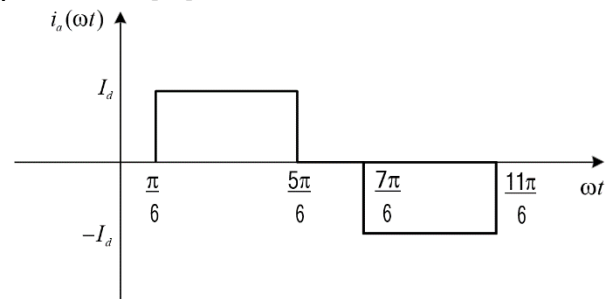


Figure 1. The current of one of the phases of the BLDC motor

In general, there are two different methods to reduce torque ripple. The first method is the optimal design of the motor structure [11-15] and the other method is the use of an advanced control strategy in the operation of the motor feeding current.

If the motor structure without groove and with surface iron is selected, the only component of the ripple torque that is related to the motor structure is the non-ideality of the anti-motor voltage. For the PMSM motor, a special shape is considered for the magnets, which leads to the generation of the voltage against the sinusoidal induction motor, and the ripple torque decreases. It will be investigated in Figure 1 based on optimal design. In this motor, there is a winding wire with a full step and it is of foot type.

In section 2, the electromagnetic torque is presented using analytical relations based on anti-motor voltage and motor

feeding current. In section 3, the anti-motive voltage caused by the magnetic flux density of the magnets has been calculated and the magnetic flux density of the magnets has been calculated using Maxwell's equations and geometric mapping. In section 4, the ripple torque relationship is presented, the effect of different motor parameters on it is examined and the optimal values related to the motor structure are obtained. Finally, in section 5, the conclusion is presented.

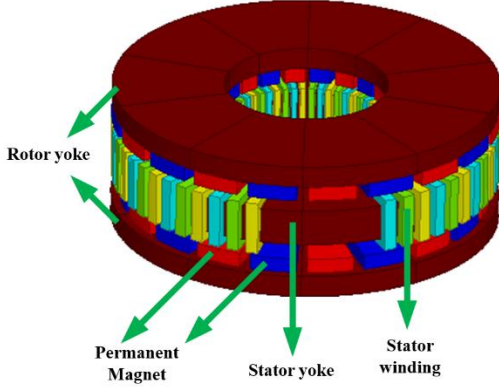


Figure 2. The structure of the middle stator without the groove of the axial permanent magnet motor

Calculation of Electromagnetic Torque using Analytical Relations

Using the Lorentz force theory, the electromagnetic torque of the motor can be expressed as follows based on the anti-motor voltage and the current of the phases [10]:

$$T(t) = \frac{1}{2\pi n} (e_a(t)i_a(t) + e_b(t)i_b(t) + e_c(t)i_c(t)) \quad (1)$$

where $e_a(t)$, $e_b(t)$, and $e_c(t)$ are the voltage of each phase, $i_a(t)$, $i_b(t)$, and $i_c(t)$ are the current of each phase and n is the rotational speed in radian per second. By having the waveform of the anti-motor voltage of each phase, its Fourier series can be written, which can be expressed as the following relation for phase a due to the symmetry of the half-wave:

$$e_a(t) = E_1 \sin(\omega t) + E_3 \sin(3\omega t) + \dots \quad (2)$$

where E_1 and E_3 are the amplitude of the harmonics of the voltage of phase (a) and ω is the angular frequency.

In a BLDC motor, the connection of the stator coils is usually star-shaped. The feeding current can also be written as a set of sinusoidal currents using the Fourier series, which is related as follows for phase a with star connection.

$$i_a(t) = i_1 \sin(\omega t) + i_3 \sin(3\omega t) + \dots \quad (3)$$

where i_1 and i_2 are the range of harmonics of phase (a) current.

In the BLDC motor, the current of each phase is rectangular and with 120 degrees of electrical conduction in each half cycle. Figure 2 shows the flow of phase (a) of the BLDC motor. According to Figure 2, the Fourier series of phase a current corresponds to the following relation:

$$i_a(\omega t) = \frac{4}{\pi} I_d \sum_{n=1,3,5}^{\infty} \frac{1}{n} \cos\left(\frac{n\pi}{6}\right) \sin(n\omega t) \quad (4)$$

Due to the existing symmetry in the motor, the anti-motor voltage and current of phases b and c have a phase difference of 120 compared to phase a. Assuming that the supply current and the anti-motor voltage of each phase

are in phase, the electromagnetic torque can be calculated from (1), which is expressed as follows by performing mathematical calculations [6]:

$$T_{em}(t) = T_{avg} + \sum_{n=1,3,5}^{\infty} T_{6n} \cos(6n\omega t) \quad (5)$$

Where T_{avg} is the average torque or useful torque of the BLDC motor and corresponds to the following relationship:

$$T_{avg} = \frac{3}{2\omega_m} (E_1 I_1 + E_5 I_5 + E_7 I_7 + \dots) \quad (6)$$

In (5), T_{6n} is the range of torque harmonics, which leads to the generation of torque ripple. The values of T_6 , T_{12} , T_{18} , T_{24} , and T_{30} are calculated according to the following relationships:

$$T_6 = \frac{2}{2\omega_m} (I_1(E_7 - E_5) + I_5(E_{11} - E_1) + \dots) \quad (7)$$

$$T_{12} = \frac{2}{2\omega_m} (I_1(E_{13} - E_{11}) + I_5(E_{17} - E_5) + \dots) \quad (8)$$

$$T_{18} = \frac{2}{2\omega_m} (I_1(E_{19} - E_{17}) + I_5(E_{23} - E_{13}) + \dots) \quad (9)$$

$$T_{24} = \frac{2}{2\omega_m} (I_1(E_{25} - E_{23}) + I_5(E_{29} - E_{19}) + \dots) \quad (10)$$

$$T_{30} = \frac{2}{2\omega_m} (I_1(E_{31} - E_{29}) + I_5(E_{35} - E_{25}) + \dots) \quad (11)$$

By having different harmonics of the supply current and counter voltage of the BLDC motor, the average torque and different harmonics of the electromagnetic torque can be calculated based on the above relationships. Current harmonics are obtained from (4). The harmonics of the anti-motor voltage can be calculated using the analytical method presented in the next section.

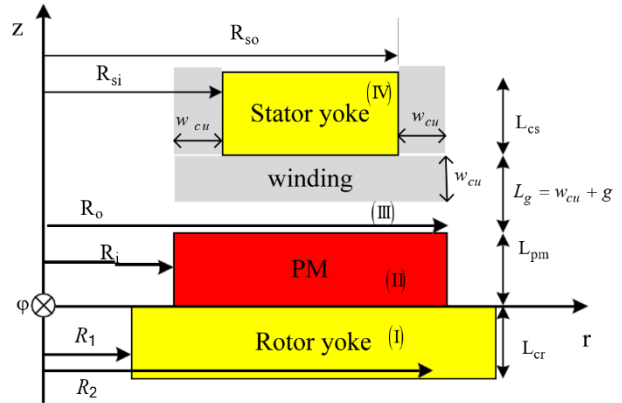


Figure 3. Different areas of BLDC motor

Calculating the Power of the Induction Electric Motor using Analytical Relations

By having the distribution of magnetic flux density and harmonics related to it, different harmonics of anti-motor voltage in BLDC motor can be calculated according to (12):

$$V_{n,rms} = \sqrt{2} \pi n N_{ph} (R_o^2 - R_i^2) B_{n,eff} \quad (12)$$

Where N_{ph} is the number of windings turns of each phase, n is the angular speed in terms of revolutions per second and R_i , R_o are the inner and outer radii of the conductors, respectively. Also $B_{n,eff}$ it is the average domain of the magnetic flux density caused by the magnets in the winding region. The average $B_{n,eff}$ value of the harmonic domain n is the magnetic flux density in different radii and

at different heights of the winding region, which can be calculated from the following relationship:

$$B_{n,eff} = \frac{1}{z_2 - z_1} \times \frac{1}{R_o - R_i} \int_{z_1}^{z_2} \int_{R_i}^{R_o} B_n dr dz \quad (13)$$

where z_1 and z_2 are the winding areas in the axial direction and B is the magnetic flux density related to the n -th harmonic caused by the conductors in different places of the winding region, which can be calculated analytically. In continuation, by using the geometric map and Maxwell's equations, a three-dimensional analytical method is presented for calculating the magnetic flux density caused by the conductors in the air gap and in the area of the coils. Then, using it, the magnetic flux density is calculated.

Considering the symmetry in the geometry of the motor (Figure 1), in order to calculate the magnetic flux density in the air gap, the machine is divided into two separate sections, the lower half of the machine is presented in Figure 3. In this figure, the motor is divided into four areas. Area (I) includes the rotor yoke, area (II) includes the magnets, area (III) is the distance between the magnets to the stator yoke, which includes the aerial distance and armature winding, and finally area (IV) which includes the stator yoke.

$$R_{so} = R_o - w_{cu} \quad (14)$$

$$R_{si} = R_i + w_{cu} \quad (15)$$

In order to calculate the magnetic flux density, first by using the geometric mapping, the magnets have been changed from a polar shape to a rectangular shape in a new page, and then by using the solution of Laplace's equation and the calculation of the scalar magnetic potential, the flux density is calculated in magnitude. Figures 4 and 5 show the maps made on the polar plate including the magnets and the conversion of radial magnets to rectangular magnets with related maps. In Figure 4, using the map $T = \ln Z$, the shape of the magnets changes from a radial form to a rectangular form. The length of all the iron bars in the new page is constant and equal to $\ln R_i - \ln R_o$ and the width of all the iron bars in the new page is also constant and equal to $\alpha_p(\pi/p)$. In Figure 5, using the map $W = R_b \times (T - R_a)$, The rebars have been moved to the center of the vertical axis. Also, their length and width units have been changed according to the length units. R_a and R_b are defined as the following relations.

$$R_a = \frac{\ln R_o - \ln R_i}{2} \quad (16)$$

$$R_b = \frac{R_o - R_i}{\ln R_o - \ln R_i} \quad (17)$$

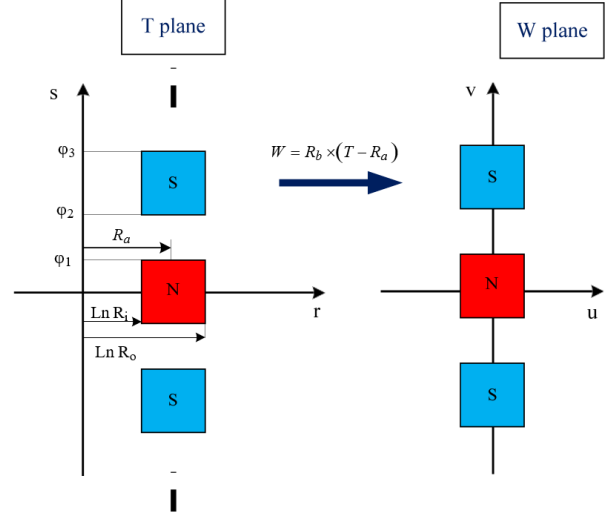


Figure 5. Magnets mapping in the second step

Figure 6 shows one of the magnets before and after mapping. In the direction of the v axis, the magnetization vector is alternating with the period of $2\pi R_b/p$ and in the direction of the u axis, it can be artificially considered to be alternating with the period of $4u_2$. The values u_1 and u_2 are in the form of the following relationships:

$$u_1 = \frac{R_o - R_i}{2} \quad (18)$$

$$u_2 = \frac{R_o - R_i}{2} \times \frac{\ln R_2 - \ln R_1}{\ln R_o - \ln R_i} \quad (19)$$

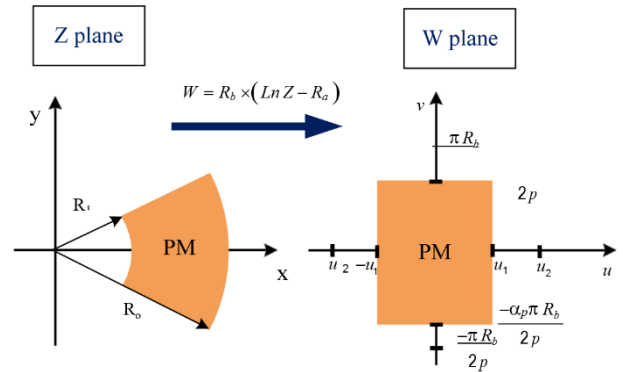


Figure 6. The mapping done on the Magnets

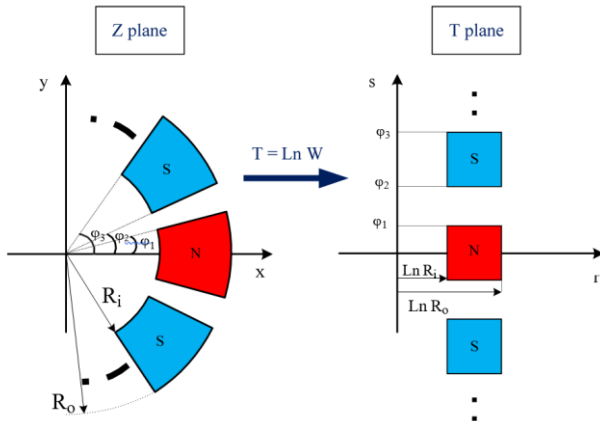


Figure 4. Magnets mapping in the first step

The magnets used in the slot less structure of the BLDC motor must have a high energy density to provide the desired magnetic flux density. For this purpose, you can use NdFeB magnets, which have high energy density. In this type of irons, the demagnetization characteristic in the second region is linear and the following relationship can be expressed for the magnetic flux density based on the magnetization vector and the magnetic field intensity [24]:

$$\vec{B} = \vec{B}_r + \mu \vec{H} = \mu_0 \vec{M} + \mu \vec{H} \quad (20)$$

$$\vec{M} = M_z(u, v) \hat{a}_z \quad (21)$$

Where B_r is the residual flux density of the magnets, H is the magnetic field strength, μ is the magnetic permeability coefficient of the magnets, μ_0 is the magnetic permeability coefficient in vacuum and M is the magnetization vector

which in the rails used in spindle machines only have components in the horizontal direction. Different components of the magnetic field are related to the scalar magnetic potential using the following relationships [23]:

$$H_u = \frac{\partial V_m(u, v, z)}{\partial u} \quad (22)$$

$$H_v = \frac{\partial V_m(u, v, z)}{\partial v} \quad (23)$$

$$H_z = \frac{\partial V_m(u, v, z)}{\partial z} \quad (24)$$

Where V_m is the scalar magnetic potential. The magnetization vector can be expanded using the double Fourier series, which will be as (25):

$$M_z(u, v) = \sum_{m=1}^{\infty} \sum_{n=1}^{\infty} M_{nm} \cos(\omega_n u) \cos(\omega_m v) \quad (25)$$

That, we have:

$$M_{nm} = \frac{16}{nm\pi^2} \frac{B_r}{\mu_0} \sin(\omega_n u_1) \sin\left(\omega_m \frac{\alpha_p \pi}{2p}\right) \quad (26)$$

$$\omega_m = \frac{mp}{R_b} \quad (26)$$

$$\omega_n = \frac{n\pi}{2u_2} \quad (26)$$

Due to the absence of current in the no-rain condition, the scalar magnetic potential is true in Laplace's equation [23]. According to the completed maps, Laplace's equation must be solved in Cartesian coordinates. Laplace's equation in Cartesian coordinates with u , v , and z components is related as follows

$$\frac{\partial^2 v_m}{\partial^2 u} + \frac{\partial^2 v_m}{\partial^2 v} + \frac{\partial^2 v_m}{\partial^2 z} = 0 \quad (27)$$

Using the method of separation of variables, the general answer of Laplace's equation in region (II) and (III) is in the form of the following relations:

$$V_{m2}(u, v, z) = \sum_{m=1,3,5}^{\infty} \sum_{n=1,3,5}^{\infty} A_1 \sinh(kz) \cos(\omega_n u) \cos(\omega_m v) \quad (28)$$

$$V_{m3}(u, v, z) = \sum_{m=1,3,5}^{\infty} \sum_{n=1,3,5}^{\infty} A_2 \sinh(k(z - L_g)) \cos(\omega_n u) \cos(\omega_m v) \quad (29)$$

Where L_g is the distance from the surface of the iron to the surface of the stator yoke. The coefficients ω_n and ω_m are in the form of (26) and the coefficient k corresponds to the following relationship:

$$k = \sqrt{\omega_n^2 + \omega_m^2} \quad (30)$$

To obtain the coefficients A_1 and A_2 in the potential equation, boundary conditions must be used.

Due to the absence of current in the border between areas (II) and (III), the tangential components of the electric field intensity are equal, which leads to the following relationships.

$$\frac{\partial V_{m2}}{\partial u} \Big|_{z=L_{pm}} = \frac{\partial V_{m3}}{\partial u} \Big|_{z=L_{pm}} \quad (31)$$

$$\frac{\partial v_{m2}}{\partial v} \Big|_{z=L_{pm}} = \frac{\partial v_{m3}}{\partial v} \Big|_{z=L_{pm}} \quad (32)$$

The vertical components of the magnetic flux density are also equal, which causes the following boundary condition.

$$-\mu_0 \mu_r \frac{\partial V_{m2}}{\partial z} + M_z \Big|_{z=L_{pm}} = -\mu_0 \frac{\partial v_{m3}}{\partial z} \Big|_{z=L_{pm}} \quad (33)$$

By specifying the coefficients A_1 and A_2 , the scalar magnetic potential in the region (II) and (III) is obtained, and finally, having the scalar magnetic potential, the axial component of the magnetic flux density in the air distance can be calculated from the following relationship

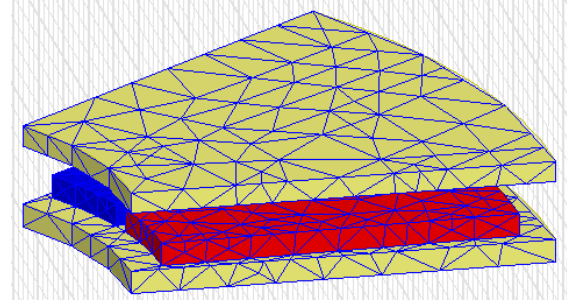


Figure 7. Meshing a pair of poles from the machine in the finite element software

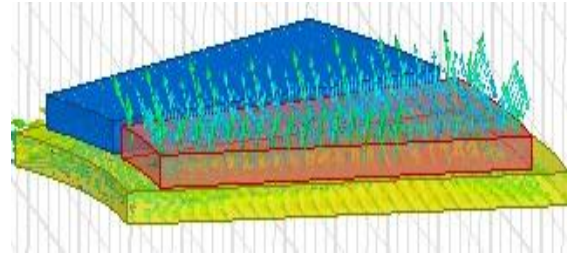


Figure 8. Distribution of the magnetic flux density vector in the magnets and the rotor yoke

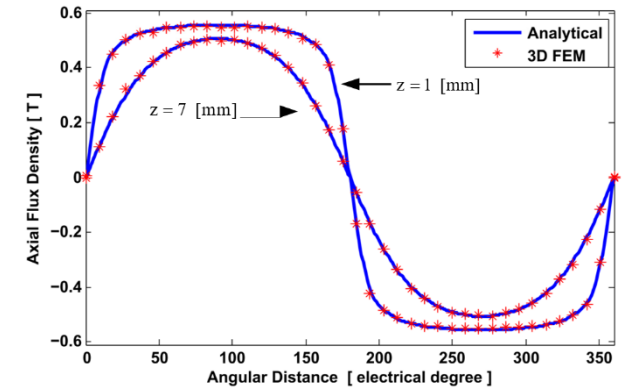


Figure 9. Axial component of magnetic flux density caused by magnets according to electric angle in one pole step

$$B_{z3} = -\mu_0 \frac{\partial V_{m3}}{\partial z} \quad (34)$$

Having B_{z3} and averaging it in the winding region, it is possible to calculate the anti-motor voltage and its harmonics in the stator windings using (12). To confirm the presented analytical method, finite element software was used and BLDC motor specifications are given in Table 1. Figure 7 shows the meshing of a pair of poles of the considered machine in Maxwell Ansoft finite element software and Figure 8 shows the magnetic flux density vector on the surface of the magnets.

Figure 9 shows the axial component of the magnetic flux density according to the electric angle in one pole step. The axial component of the magnetic flux density for different distances from the surface of the magnets has been drawn in the average beam and the distance from the surface of the magnets has been determined with the variable z . The axial magnetic flux density in the vicinity of the magnets has a trapezoidal state, and with the

distance from the surface of the magnets, it is close to the surface of the stator core. The sinusoidal shape is approaching.

Table 2 shows the effective value of anti-motive voltage obtained from the analytical method presented in this article and the value obtained using three-dimensional finite element software. Table 3 shows the different average harmonics of the magnetic flux density in the winding region and the corresponding harmonics of the counter-motive voltage that can be calculated from (12).

Table 1: Characteristics of BLDC motor

Specifications	Symbol	Value [unit]
The number of pairs of poles	p	10
The density of the rest of the magnets	B _r	1.23 [T]
Relative permeability coefficient of magnets	μ _r	1.05 [mm]
The thickness of iron	L _{pm}	6.5 [mm]
The outer beam of irons	R _o	125 [mm]
The inner beam of the irons	R _i	61 [mm]
The average beam of ironworkers	R _g	93 [mm]
The outer radius of the iron rotor	R ₂	131 [mm]
Inner diameter of iron rotor	R ₁	55 [mm]
Outer beam of iron stator	R _{so}	119 [mm]
Inner diameter of stator iron	R _{si}	67 [mm]
Rotor yoke thickness	L _{cr}	6 [mm]
Stator yoke thickness	L _{cs}	13 [mm]
The development of screws	w _{cu}	6 [mm]

Table 2: The voltage caused by analytical method and finite element

	Analytical method	Finite element
Voltage	34.6 [V]	34.9 [V]

Table 3: Different harmonics of magnetic flux density and counter-motive voltage

Harmonic order	V _{n,rms} [V]	B _{eff,n} [T]
1	34.1818	0.5400
3	5.3068	0.0838
5	1.6097	0.0254
7	0.6280	0.0099
9	0.2704	0.0043
11	0.1177	0.0019
13	0.0473	0.0007
15	0.0138	0.0002
17	0.0018	0.00004
19	0.0084	0.0001

Calculation of torque's Ripple

In this section, the ripple torque in BLDC motor with specifications according to Table 1 is discussed. For the ripple torque, various relations have been presented [10] and in this article the following relation has been used to calculate the ripple torque.

$$T_{ripple} = \frac{T_{max} - T_{min}}{T_{avg}} \quad (35)$$

Where T_{max} and T_{min} are the maximum and minimum values of torque moment, respectively, and T_{avg} is the average moment torque, which corresponds to (6). Figure 10 shows the ripple torque curve according to the pole arc

to pole pitch parameter in the BLDC motor with specifications according to table 1.

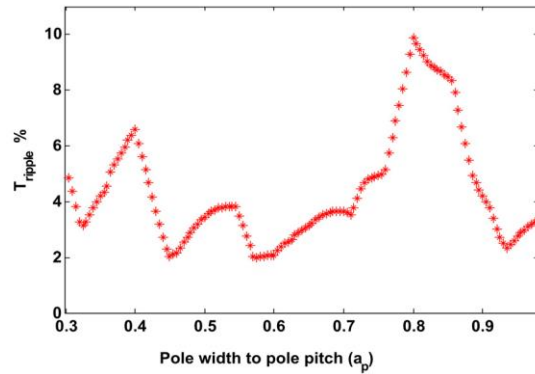


Figure 10. Ripple torque changes according to the ratio of pole arc to pole pitch in the motor

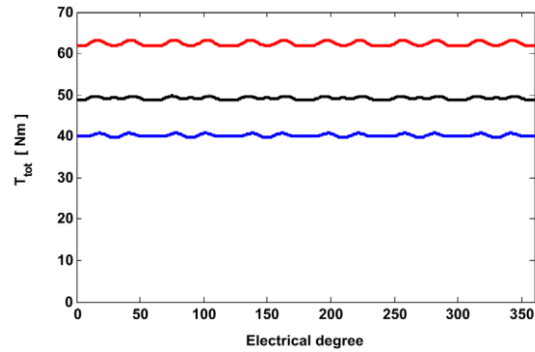


Figure 11. Electromagnetic torque of the whole motor for three different values of alpha_p.

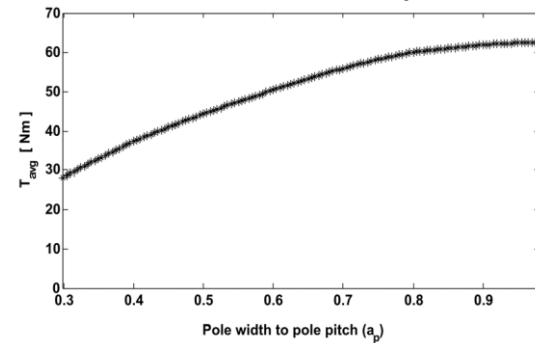


Figure 12. Average torque for different alpha_p of the motor

According to Figure 10, Ripple's torque has a minimum value in some values. The minimum value of ripple torque will occur in alpha_p=0.44, alpha_p=0.44 and alpha_p=0.44. Figure 11 shows the total electromagnetic torque according to time for three values of alpha_p where the ripple torque is minimum. As it is evident from Figure 11, the value of momentary torque in BLDC motor has the highest value for alpha_p=0.94. Figure 12 shows the average torque according to alpha_p. According to Figure 12, it can be seen that the average torque value increases with the increase of alpha_p. Figure 13 shows the changes of the ripple torque according to the air distance, and it can be seen that the minimum value of the ripple torque occurs in the air distance of about 1 mm. Figure 14 shows the diagram of ripple torque and average torque according to the ratio of inner diameter to outer diameter. According to figure 14, ripple torque has the minimum value around the ratio of diameters equal to 0.48. Figure 15 shows the ripple torque

diagram according to the number of pole pairs. According to Figure 15, the ripple torque decreases with the increase in the number of poles pairs and reaches the minimum value at $p=10$, then with the increase in the number of pole pairs, the ripple torque also increases slightly.

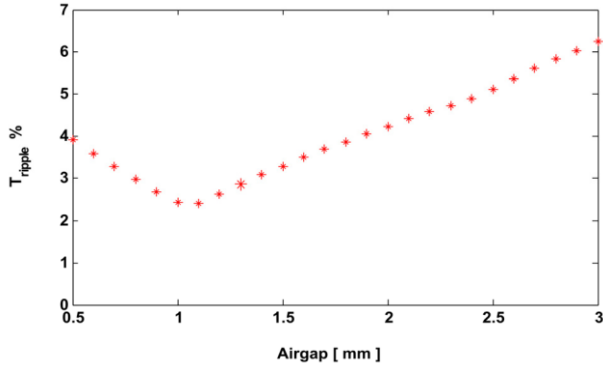


Figure 13. Ripple torque according to the length of the aerial distance

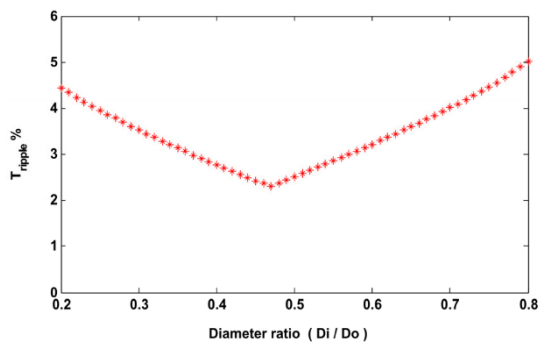


Figure 14. Ripple torque according to the ratio of inner diameter to outer diameter

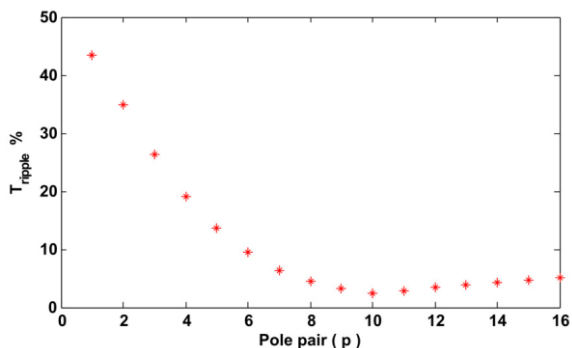


Figure 15. Ripple torque according to the number of pairs of poles

Conclusions

In this article, the electromagnetic torque of the BLDC spindle motor was obtained by using the series of current and voltage against the drive of the phases. In the operation of the counter-motive voltage of the BLDC motor, it is not a perfect trapezoid, but it is a quasi-trapezoid whose different harmonics are obtained by using analytical relations and with the help of the magnetic flux density of the air gap. The dependence of the ripple torque on the parameters related to the motor design was investigated. The parameters for which the ripple torque was evaluated were the ratio of the pole arc to the pole pitch, the length of the aerial distance, the ratio of the inner diameter to the outer diameter and the number of pairs of poles, which according to the results obtained, the values are higher for these values. The ripple torque minimum was determined.

References

- [1] P. Pillay and R. Krishnan, "Modeling, simulation, and analysis of permanent-magnet motor drives, part ii: the brushless DC motor drive," *IEEE Trans. Ind. Appl.*, vol. 25, no. 2, pp. 274-279, Mar./Apr. 1989.
- [2] A. Rubaai, A. Ofoli, and M. Castro, "dSPACE DSP-based rapid prototyping of fuzzy PID controls for high performance brushless servo drives," in the 41st IAS Annual Meeting of the IEEE Ind. Appl. Conf., IEEE Press, vol. 3, pp. 1360-1364, Oct. 2006.
- [3] A. Mousaei and M. B. B. Sharifian, "Design and optimization of a linear induction motor with hybrid secondary for textile applications," 2020 28th Iranian Conference on Electrical Engineering (ICEE), 2020, pp. 1-6, doi: 10.1109/ICEE50131.2020.9260773.
- [4] G. Mikerov Alexander, "Brushless DC torque motors quality level indexes for servo drive applications," in Proc. IEEE EUROCON 09, pp. 827-834, St.-Petersburg, Russia, 18-23 May 2009.
- [5] D. C. Hanselman, "Minimum torque ripple, maximum efficiency excitation of brushless permanent magnet motors," *IEEE Trans. Ind. Electron.*, vol. 41, no. 3, pp. 292-300, Jun. 1994.
- [6] A. Mousaei, M. B. Bannae Sharifian and N. Rostami, "Direct Thrust Force Control (DTFC) of Optimized Linear Induction Motor with Super Twisting Sliding Mode Controller (STSMC)," 2021 12th Power Electronics, Drive Systems, and Technologies Conference (PEDSTC), 2021, pp. 1-5, doi: 10.1109/PEDSTC52094.2021.9405903.
- [7] M. Aydin, S. Huang, and T. A. Lipo, "Axial flux permanent magnet disc machines: a review," in Proc. of Int. Symp. on Power Electronics, Electrical Drives, Automation and Motion, SPEEDAM'04, pp. 61-71, Jun. 2004.
- [8] M. Aydin, S. Huang, and T. A. Lipo, "Torque quality and comparison of internal and external rotor axial flux surface-magnet disc machines," *IEEE Trans. Ind. Electron.*, vol. 53, no. 3, pp. 822- 830, Jun. 2006.
- [9] C. C. Jensen, F. Profumo, and T. A. Lipo, "A low loss permanent magnet brushless DC motor utilizing tape wound amorphous iron," *IEEE Trans. Ind. Appl.*, vol. 28, no. 3, pp. 646-651, May/Jun. 1992.
- [10] Arash Mousaei, Nasim Bahari, Guo Miehao. Artificial Neural Networks (ANN) of Proposed Linear Induction Motor with Hybrid Secondary (HLIM) Considering the End Effect. American Journal of Electrical and Computer Engineering.

Vol. 5, No. 1, 2021, pp. 32-39.
doi: 10.11648/j.ajece.20210501.15.

Trans. Power Electronics, vol. 23, no. 2, pp. 950-958, Mar. 2008.

- [11] T. M. Jahns and W. L. Soong, "Pulsating torque minimization techniques for permanent magnet AC motor drives-a review," *IEEE Trans. Ind. Electron.*, vol. 43, no. 2, pp. 321-329, Apr. 1996.
- [12] T. M. Jahns, "Torque production in permanent-magnet synchronous motor drives with rectangular current excitation," *IEEE Trans. on Ind. Appl.* vol. 20, no. 4, pp. 803-813, Jul./Aug. 1984.
- [13] P. Upadhyay and K. R. Rajagopal, "Torque ripple minimization of interior permanent magnet brushless DC motor using rotor pole shaping," in *Proc. IEEE Power Electronics, Drives and Energy Systems, PEDES'06*, IEEE Press, 3 pp., 12-15 Dec. 2006.
- [14] L. Parsa and H. Lei, "Interior permanent magnet motors with reduced torque pulsation," *IEEE Trans. Ind. Electron.*, vol. 55, no. 2, pp. 602-609, Feb. 2008.
- [15] D. H. Wang, X. H. Wang, and T. T. Ding, "Optimization for the asymmetric angles of magnetic pole to reduce cogging torque in inner-buried PM brushless DC motors," *Proceedings of the CSEE*, vol. 28, no. 9, pp. 66-70, Mar. 2006.
- [16] M. S. Islam, S. Mir, and T. Sebastian, "Design considerations of sinusoidally excited permanent magnet machines for low-torque-ripple applications," *IEEE Trans. on Ind. Appl.*, vol. 41, no. 4, pp. 955-962, Jul./Aug. 2005.
- [17] F. Song, B. Zhou, and X. Q. Wu, "Novel compensation method to suppress commutation torque ripple for brushless DC motor," *Trans. of China Electrotechnical Society*, vol. 23, no. 11, pp. 28-33, Nov. 2008.
- [18] Y. Liu, Z. Q. Zhu, and D. Howe, "Commutation-torque-ripple minimization in direct-torque-controlled PM brushless DC drives," *IEEE Trans. Industry Applications*, vol. 43, no. 4, pp. 1012-1021, Jul./Aug. 2007.
- [19] P. Lin, K. Wei, and Z. C. Zhang, "A novel control scheme to suppress the commutation torque ripple in BLDCM," in *Proc. of the CSEE*, vol. 26, no. 3, pp. 153-158, Feb. 2006.
- [20] K. Y. Nam, W. T. Lee, and C. M. Lee, "Reducing torque ripple of brushless DC motor by varying input voltage," *IEEE Trans. Magnet.*, vol. 42, no. 4, pp. 1307-1310, Apr. 2006.
- [21] H. F. Lu, L. Zhang, and W. L. Qu, "A new torque control method for torque ripple minimization of BLDC motors with un-ideal back EMF," *IEEE Trans. Power Electronics*, vol. 23, no. 2, pp. 950-958, Mar. 2008.
- [22] P. R. Sultana and P. L. Pathi, "Minimization of torque ripples in BLDC motor using PWM technique," *International Journal of Advanced Research in Electrical, Electronics and Instrumentation Engineering*, vol. 3, no. 9, pp. 12043-12050, Sep. 2014.
- [23] T. Chan, L. Lai, and S. Xie, "Field computation for an axial flux permanent-magnet synchronous generator," *IEEE Trans. on Energy Conversion*, vol. 24, no. 1, pp. 1-11, Mar. 2009.
- [24] Y. Huang, B. Ge, J. Dong, H. Lin, J. Zhu, and Y. Guo, "3-D analytical modeling of no-load magnetic field of ironless axial flux permanent magnet machine," *IEEE Trans. on Magnet.*, vol. 48, no. 11, pp. 2929-2932, Nov. 2012.